### Title

High-contrast osteochondral junction imaging using a 3D dual adiabatic inversion recovery-prepared ultrashort echo time cones sequence




### Journal

NMR in Biomedicine, 34(8)

### ISSN

0952-3480



### Authors

Lombardi, Alecio F
Jang, Hyungseok
Wei, Zhao
et al.



### Publication Date

2021-08-01

### DOI

10.1002/nbm.4559

Peer reviewed

HHS Public Access

Author manuscript

*NMR Biomed*. Author manuscript; available in PMC 2022 August 01.

Published in final edited form as:

*NMR Biomed*. 2021 August ; 34(8): e4559. doi:10.1002/nbm.4559.

# High-Contrast Osteochondral Junction Imaging Using a 3D Dual Adiabatic Inversion Recovery Prepared Ultrashort Echo Time (3D DIR-UTE) Cones Sequence

**Alecio F. Lombardi**[1,2], **Hyungseok Jang**[1], **Zhao Wei**[1], **Saeed Jerban**[1], **Mark Wallace**[3], **Koichi Masuda**[4], **Ya-Jun Ma**[1]

[1]Department of Radiology, University of California, San Diego, CA

[2]Research Service, Veterans Affairs San Diego Healthcare System, San Diego, CA

[3]Department of Anesthesiology, University of California San Diego, La Jolla, CA

[4]Department of Orthopedic Surgery, University of California San Diego, La Jolla, CA

## Abstract

**Background:** While conventional MRI sequences cannot visualize tissues from the osteochondral junction (OCJ) due to these tissues' short transverse $T_2$/$T_2$* relaxations, ultrashort echo time (UTE) sequences can overcome this limitation. A 2D UTE sequence with a dual adiabatic inversion recovery preparation (DIR-UTE) for selective imaging of short $T_2$ tissues with high contrast has previously been developed, but high sensitivity to eddy currents and aliased out-of-slice excitation make it difficult to image the thin layer of the OCJ in vivo. Here, we combine the DIR scheme with a 3D UTE Cones sequence for volumetric imaging of OCJ tissues in vivo, aiming to generate higher OCJ contrast compared with a recently developed single IR-prepared UTE sequence with a fat saturation module (IR-FS-UTE).

**Methods:** All sequences were implemented on a 3T clinical scanner. The DIR-UTE Cones sequence combined a 3D UTE Cones sequence with two narrow-band adiabatic IR preparation pulses centered on water and fat spectrum frequencies, respectively. The 3D DIR-UTE Cones sequence was first applied to a phantom, then to the knees of four healthy volunteers and four patients diagnosed with osteoarthritis and compared to the IR-FS-UTE sequence.

**Results:** In both phantom and volunteer studies, the proposed DIR-UTE Cones sequence showed much higher contrast for OCJ imaging than the IR-FS-UTE sequence did. The 3D DIR-UTE Cones sequence showed a significantly higher contrast-to-noise ratio (CNR) between the OCJ and subchondral bone fat (BF) (mean, standard deviation (SD): 25.7 ± 2.3) and between the OCJ and superficial layers of cartilage (SC) (mean, SD: 22.2 ± 3.5) compared to the IR-FS-UTE sequence (mean, SD: 10.8 ± 2.5 and 16.3 ± 2.6, respectively).

Corresponding author: Ya-Jun Ma, Ph.D., yam013@ucsd.edu, University of California, San Diego, La Jolla, CA 92037, Phone: (858) 246-2299.

Declaration of Competing Interest

The authors have no conflicts of interest to declare.

Data Availability

The data that support the findings of this study are available from the corresponding author upon reasonable request.

**Conclusions:** The 3D DIR-UTE Cones sequence is feasible for imaging of the OCJ region of the knee in vivo and produces both high resolution and high contrast.

## Graphical Abstract

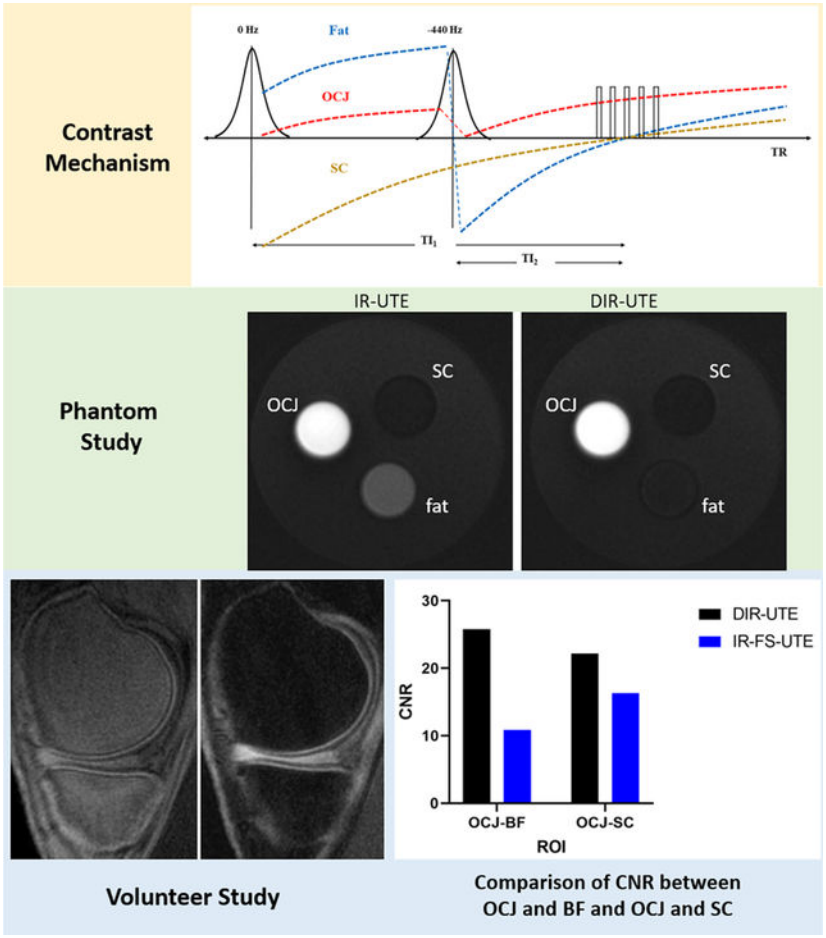


A DIR-UTE Cones sequence combining a 3D UTE Cones sequence with two narrow-band adiabatic IR preparation pulses centered on water and fat spectrum frequencies was implemented and applied to a phantom, to the knees of four healthy volunteers and four patients with osteoarthritis and compared to an IR-FS-UTE sequence. The proposed DIR-UTE Cones sequence showed higher contrast-to-noise ratio between osteochondral junction and bone marrow fat and between osteochondral junction and superficial cartilage in both phantom and in vivo knee studies.

### Keywords

Osteochondral junction; dual adiabatic inversion recovery; ultrashort echo time

## 1. Introduction

According to the latest Global Burden of Disease Study in 2017, musculoskeletal disorders are the primary cause of years lived with disability (YLDs) worldwide (1). From 2000 to 2015 alone, the total number of YLDs among musculoskeletal disorders increased by 34.2%

(2). Osteoarthritis (OA) is the second most common contributor to this burden and affects around 303 million people around the world (1, 3).

Osteoarthritis can affect any joint, but preferentially affects the knee, hands, hip, and spine (3). It is a multifactorial disease with different pathophysiological pathways involving ligaments, meniscus, synovium, subchondral bone, and cartilage (4). The osteochondral junction (OCJ), that anchors the cartilage to the subchondral bone thus distributing the joint's mechanical load, may play a particular role in the initiation and progression of OA (5–8). Comprised of the deepest layer of non-calcified cartilage, the layer of calcified cartilage, and the subchondral plate of lamellar bone (5), the OCJ may be associated with a series of processes that lead to joint inflammation, cartilage damage, and bone remodeling (7–10).

MRI is the most sensitive imaging modality available for detecting OA in its early stages (11, 12), but conventional MRI sequences cannot visualize tissues from the OCJ due to the tissues' short transverse $T_2$/$T_2$* relaxations (13, 14). Ultrashort echo time (UTE) sequences with echo times lower than 100 μm can overcome this limitation (15, 16). A few UTE sequences have been developed to study the OCJ region, including UTE dual-echo subtraction and inversion recovery (IR)-prepared UTE techniques (16–20). UTE dual-echo acquisition is time-efficient but suffers from a low contrast-to-noise ratio (CNR) between the OCJ and subchondral bone fat (BF) (17). The high proton density and relatively short $T_2$* from BF showed high signal intensity after echo subtraction, reducing the contrast between the OCJ and BF (21). On the other hand, a more recently developed single IR-prepared UTE sequence incorporated with a fat saturation module (IR-FS-UTE) was proposed to suppress signals from both superficial layers of cartilage (SC) and BF to highlight the OCJ region (20). When combined with 3D sequences for high-resolution OCJ imaging, a multi-spoke acquisition strategy was employed to reduce total scan time (20). However, the fat suppression efficiency decreases significantly as the number of spokes in each TR increases. This resulted in a compromise between fat suppression and scan time.

Ten years ago, investigators developed a 2D UTE sequence with a dual adiabatic inversion recovery preparation (DIR-UTE) for selectively imaging short $T_2$ tissues (18). Two IR pulses with on-resonance frequencies centered on water and fat were used to suppress SC and BF signals, respectively (16). However, this 2D DIR-UTE sequence has mainly been applied for ex vivo small sample imaging since the sequence is sensitive to eddy currents and suffers from aliased out-of-slice excitation, making it difficult to image the thin layer of the OCJ region in vivo (22). The present study combined the DIR scheme with a 3D UTE Cones sequence (DIR-UTE Cones) for high-resolution and high-contrast imaging of OCJ tissues in vivo. The multi-spoke acquisition strategy was employed in the 3D DIR-UTE Cones sequence to reduce the total scan time, facilitating its practical use in the clinical setting. The IR-FS-UTE Cones sequence was also used for comparison. Both sequences were acquired with the same scan time. We expected that the proposed 3D DIR-UTE Cones sequence generated a high OCJ contrast better than the IR-FS-UTE Cones, especially between OCJ and BF.

## 2. Material and Methods

### 2.1 MR Acquisition and pulse sequence

Our institutional review board approved this study. All sequences were implemented on a 3T MR750 scanner (GE Healthcare Technologies, Milwaukee, WI, USA) and an eight-channel transmit/receive knee coil was used for in vivo whole knee joint imaging.

The DIR-UTE Cones sequence combined a 3D UTE Cones sequence with two adiabatic IR preparation pulses (duration = 20 ms and bandwidth = 500 Hz) (23), and a series of spokes (i.e., $N_{sp}$), acquired after each DIR preparation to accelerate the scan (Figure 1). A short time period ($\tau$) was applied between each spoke. For each spoke, a short rectangular pulse (e.g., 50 μs) was used for non-selective signal excitation so that no slab selection gradient-related eddy currents were introduced to the subsequent spiral trajectory data acquisition with conical view ordering. Data sampling began from the center of the k-space and continued outwards and was begun as soon as was practical after the radiofrequency (RF) excitation, with a minimal nominal delay time of 32 μs. Both RF and gradient spoiling were used to crush the residual transverse magnetizations.

### 2.2 Contrast Mechanism

Initially, the magnetizations of the SC (long $T_1$ and $T_2$) and the BF (short $T_1$ and relatively long $T_2$) were inverted by two narrow-band adiabatic IR pulses (Figure 1). These pulses were centered on the spectrum frequencies of water and fat, respectively, and were applied at different times so that they could both reach the nulling point at the time of data acquisition (16). In contrast, the short $T_2$ magnetization of the OCJ could not be fully inverted by the relatively long adiabatic IR pulses and was instead mostly saturated during these pulses, meaning that the magnetization of OCJ recovered from zero. When the DIR-UTE Cones acquisition started around the nulling point of the SC and BF, the OCJ presented with high signal and was therefore highlighted (Figure 1).

### 2.3 Phantom Study

The 3D DIR-UTE Cones sequence was applied to a phantom (Figure 2) comprised of a tube of vegetable oil ($T_1$ ~ 260 ms; simulating BF), a tube of distilled water containing $MnCl_2$ (0.015 g/L, $T_1$ ~ 900ms; $T_2$ ~ 120ms, simulating SC), and a tube of distilled water containing $MnCl_2$ in a different concentration (3.6 g/L, $T_1$ < 30ms; $T_2$ ~ 0.5ms, simulating OCJ), all in a container filled with agarose gel ($T_1$ ~ 2600ms; $T_2$ > 150ms). The $T_1$ values of the $MnCl_2$ solutions, vegetable oil, and agarose gel were assessed using the 3D UTE Cones actual flip angle and variable flip angle sequences that have been previously described (24, 25).

For comparison, 3D fast spoiled gradient echo (FSPGR) and four additional 3D UTE protocols were applied: the IR-FS-UTE Cones, a proton density-weighted UTE ($PD_w$-UTE) Cones with fat saturation (FatSat), a $PD_w$-UTE Cones without FatSat, and a $T_1$-weighted UTE ($T_{1w}$-UTE, with a high flip angle and a short TR) Cones. The imaging parameters are listed in Table 1. The same TR was employed in both IR-FS-UTE and DIR-UTE Cones sequences, while the optimal TIs in the IR-FS-UTE and DIR-UTE Cones sequences were

determined experimentally ($TI_1/TI_2$ for DIR-UTE = 400/160 ms; TI for IR-UTE = 160 ms). Both IR-FS-UTE and DIR-UTE Cones sequences were acquired with the same scan time.

### 2.4 In vivo knee study in healthy volunteers

Following the phantom study, 3D DIR-UTE Cones ($TR/TI_1/TI_2$ = 1200/520/180 ms), FSPGR (TE = 2.4 ms), IR-FS-UTE Cones (TR/TI = 1200/600 ms), and clinical 2D $T_2$-weighted fast spin-echo ($T_{2w}$-FSE) (TR/TE = 4400/102 ms) sequences were performed in four knee joints from four healthy volunteers (ranging from 33 to 47 years old, males) and four patients with a diagnosis of osteoarthritis (49 to 61 years old, males). Informed consent was obtained from all volunteers per the guidance of our institutional review board approval. The detailed image parameters are listed in Table 2. The TR and TI used in the IR-FS-UTE sequence were identical to those used in a previous study (20), while the TR that was used in the DIR-UTE Cones sequence was the same as that which was used in the IR-FS-UTE Cones sequence. The optimal TIs in the DIR-UTE Cones sequences were determined experimentally ($TI_1/TI_2$ for DIR-UTE = 520/180 ms; TI for IR-UTE = 600 ms).

### 2.5 In Vivo Comparison Study between IR-based UTE sequences and $T_1$w-UTE and UTE dual echo subtraction

A comparison study was performed in the knee of one healthy volunteer (38 years old male) between the IR-based UTE techniques (DIR and IR-FS) and the more time-efficient $T_1$w-UTE and UTE dual-echo subtraction techniques. Two different datasets were acquired for the $T_{1w}$-UTE and UTE dual-echo subtraction sequences: one with the same resolution as the IR sequences and another one with higher resolution. The imaging parameters used in the $T_{1w}$-UTE and UTE dual-echo subtraction sequences are listed in Table 3.

### 2.5 Image analysis

CNRs between the OCJ and SC ($CNR_{OCJ\text{-}SC}$) and between the OCJ and BF ($CNR_{OCJ\text{-}BF}$) were calculated as the signal differences between these regions divided by the background noise. Each region's signal intensity was measured inside a region of interest (ROI) drawn by one of the investigators, a fellowship-trained musculoskeletal radiologist with seven years of experience. The noise was calculated as the standard deviation (SD) of the signal inside an ROI placed in an artifact-free image background. Descriptive statistics were performed, and the mean and standard deviation were measured to compare the CNR between the SC, OCJ, and the BF.

## 3. Results

In the phantom study, the FSPGR clinical sequence (Figure 2A) could not detect the signal from the tube which represented the OCJ. The PDw-UTE images, however, show a bright signal from the tube representing the OCJ (Figures 2B and 2C), demonstrating that the UTE sequence adequately captures signal from the OCJ, with a lower fat signal when the fat saturation module was on. The tubes representing the OCJ and fat appeared in the $T_{1w}$-UTE Cones image with higher signal intensities (Figure 2D) than those from the tube representing the SC because of the former's much shorter $T_1$ values. As can be seen in the images of Figures 2E and 2F, the signals from the tube representing the SC were well-suppressed by

the IR pulse used in the IR-FS-UTE and by the first IR pulse used in the DIR-UTE Cones sequences, indicating that the IR pulse suppressed tissue signals effectively. Meanwhile, the tube representing fat showed with relatively high signal intensity in the IR-FS-UTE Cones images, showing that the FatSat module used in the IR-FS-UTE Cones sequence only partially suppressed fat signal (Figure 2E). In comparison, the signal from the tube representing fat was well-suppressed by the second IR pulse in the DIR-UTE Cones sequence (Figure 2F), demonstrating that the IR pulse was more effective in fat suppression than the fat saturation module when using multispoke acquisition. The phantom results demonstrate that the DIR-UTE Cones sequence can highlight OCJ with effective signal suppression for both SC and fat.

Figure 3 shows the knee images from two healthy volunteers. As expected, on the clinical sequences ($T_{2w}$-FSE and FSPGR), the signal in the OCJ could not be effectively detected due to its fast signal decay. Using the IR-FS-UTE Cones sequence, the SC signal was well-suppressed to highlight the OCJ, but the BF still appeared with relatively high signal. The DIR-UTE Cones suppressed both the SC and BF signals, increasing the contrast between these tissues and the OCJ, as was the case in the phantom study, as shown in Figure 2. Supplemental Figure 1 shows all the DIR-UTE Cones images acquired from one of the volunteers. The OCJ tissues are well-visualized in the non-curved regions such as the tibial plateau, while suffering strong partial volume effect in the more curved structures such as peripheral articular surfaces. A higher resolution with isotropic data acquisition could potentially solve this problem.

In the volunteer study, the 3D DIR-UTE Cones sequence showed a significantly higher CNR between the OCJ and the BF (mean, SD: 25.7 ± 2.3) and between the OCJ and SC (mean, SD: 22.2 ± 3.5) compared to the IR-FS-UTE sequence (mean, SD: 10.8 ± 2.5 and 16.3 ± 2.6, respectively), as seen in Figure 4.

The images of OA patients in Figure 5 depict areas of deep cartilage erosions with discontinuity of the high signal from OCJ on both IR-FS-UTE and DIR-UTE Cones sequences. The DIR-UTE Cones images show better OCJ contrast than the IR-FS-UTE Cones images do.

As can be seen in Figure 6, both the IR-FS-UTE and DIR-UTE Cones sequences show much higher OCJ contrast than the $T_{1w}$-UTE and UTE dual-echo subtraction techniques, especially for the contrast between the OCJ and BF. The high resolution $T_{1w}$-UTE and UTE dual-echo sequences reduced the partial volume effect and showed a thinner OCJ structure, as expected. However, it is still difficult to distinguish the OCJ and BF with increased resolution in both the $T_{1w}$-UTE and dual-echo subtracted images.

## 4. Discussion

In this study, we showed the feasibility of using a 3D DIR-UTE Cones sequence to highlight the OCJ region in knee joints of healthy subjects and patients with OA. The shorter $T_2/T_2$* of the OCJ makes it impossible to visualize this region on regular clinical sequences, a limitation which can fortunately be overcome with UTE sequences. When paired with DIR

preparation and 3D Cones acquisition, UTE sequences can highlight the OCJ with even further improvements over the IR-FS-UTE Cones sequence due to better BF suppression. The natural short $T_1$ and $T_2$ of the OCJ region make adiabatic IR pulses highly effective in increasing contrast from these regions to the SC (20). The multi-spoke acquisition shortens the scan time (23) and the 3D acquisition increases both the (SNRs) and the resolution for effective evaluation of the OCJ region.

To accommodate the scan time and SNR, the image resolution of the current DIR-UTE Cones protocol (especially in the slice selection direction) is limited relative to the thin OCJ tissue. This leads to a partial volume effect, which artificially increases the thickness of the OCJ region in the DIR-UTE Cones image, especially in more curved structures such as peripheral articular surfaces. In addition, while the Cones trajectory was applied in this study to improve the data acquisition efficiency for UTE imaging, this twisted trajectory can lead to image blurring in tissues with short $T_2$ relaxation times, which further increases the size of the displayed OCJ region. Undersampling in the edges of k-space further reduces the image resolution. Despite the high OCJ contrast generated by the DIR-UTE Cones sequence, the blurred OCJ visualization may create difficulties in accurately measuring the size of the OCJ tissue and in detecting small morphological changes of the OCJ in clinical utilization. We would expect the image resolution of the DIR-UTE Cones sequence to increase once more advanced RF coil and gradient systems (e.g., increased gradient maximum amplitude and higher slew rate) are available in the clinical setting to provide better SNR and to shorten the encoding period, respectively.

For high contrast OCJ imaging, the IR preparation used in both the IR-FS-UTE and DIR-UTE sequences is more effective in suppressing the desired tissues with long $T_2$ relaxation times than utilizing the $T_1$ weighting in $T_{1w}$-UTE and echo signal decay in UTE dual-echo subtraction. However, the scan time of the IR-prepared UTE techniques is much longer than in the other two techniques and thus poses more restrictions in generating high image resolution and SNR for OCJ imaging.

The contrast between the OCJ and BF is low in both the $T_{1w}$-UTE and UTE dual-echo subtracted images. This is because the BF has relatively short $T_1$ and $T_2$* relaxation times, which lead to high signal (comparable with OCJ) in the $T_{1w}$-UTE and dual-echo subtracted images, respectively (20). Even with a higher resolution, it is still difficult to distinguish the OCJ and BF in both the $T_{1w}$-UTE and dual-echo subtracted images even though there is a subchondral bone plate located between them. This may be a result of the off-resonance artifacts of BF. In the non-Cartesian UTE sequence, the BF signals could shift radially into the thin subchondral bone sites (26). Since the higher resolution UTE acquisition requires even longer gradient encoding, this may further increase the off-resonance artifacts. Moreover, the stronger short $T_2$ blurring effect may also reduce the signal intensity of OCJ in these high-resolution UTE images due to the longer gradient encoding. A more powerful gradient system with increased gradient maximum amplitude and higher slew rate would be useful in shortening the encoding period, thereby reducing the off-resonance artifacts and image blurring.

Increasing evidence shows that the bright signal observed on UTE sequences mainly comes from the deep and calcified layers of cartilage (20). The SC has relatively long $T_2$ and $T_1$ values with higher water content and is suppressed by the adiabatic IR pulse with a frequency close to water. The trabecular bone has increased fat content, so it is mostly suppressed by the adiabatic IR pulse with a frequency close to fat. The subchondral bone plate contributes to the lowest signal, appearing almost as signal void because it has the lowest water content by volume (27) compared with deep and calcified layers of cartilage and also the lowest fat content due to abscense of bone marrow.

A previous study showed that the IR-FS-UTE Cones sequence could visualize the OCJ region (20), but using the 3D DIR-UTE Cones sequence adds higher contrast between the OCJ region and the subchondral bone as the adiabatic IR pulse is more effective in suppressing BF than the conventional FatSat module used on the IR-FS-UTE Cones sequence. The contrast between the OCJ and SC in DIR-UTE Cones imaging is also higher than that in the IR-FS-Cones imaging because the $TI_1$ (i.e., 540 ms) used in the DIR-UTE Cones sequence is closer to the signal nulling point of the SC than the corresponding TI (i.e., 600 ms) of the IR-FS-UTE Cones sequence. The TI with more effective SC signal nulling in the IR-UTE-Cones was not chosen for our study because we wanted a good balance of the OCJ contrast between fat and SC (20).

The performance of the DIR-UTE Cones sequence is generally more sensitive to the background magnetic field inhomogeneity than the IR-FS-UTE Cones sequence due to the limited chemical shift of marrow fat at 3T and the narrow bandwidth of the IR pulses used. Since the background field is relatively uniform in knee joints, the proposed DIR-UTE Cones can always obtain reliable OCJ imaging with high contrast. The application for other body parts, such as hip joints, may be more difficult due to the more inhomogeneous background field, a challenge which will be investigated in future studies.

For high-resolution OCJ imaging, a multi-spoke acquisition strategy was combined with the 3D sequences to reduce total scan time (23). In the IR-FS-UTE sequence, the fat suppression efficiency decreases significantly (resulting in lower contrast) as the number of spokes in each TR increases. The DIR-UTE Cones can potentially use a greater number of spokes in one TR since IR technique is more effective in fat suppression than the FatSat technique. However, if too many spokes are used for acquisition in one TR, the DIR-UTE Cones images may suffer artifacts induced by the signal variations among different acquisition spokes. In terms of scan time and image quality, a reasonable number of spokes in one TR for DIR-UTE sequence may range from 15 to 25.

Osteochondral junction alterations, specifically loss of integrity, are associated with early events in OA development and may be associated with disease progression and increased pain in osteoarthritic patients (28). The subchondral bone exposure in advanced OA is linked to an invasion of cartilage by vessels and nerves and increased endochondral ossification (29). Typically, the OCJ has a decreased amount of collagen and a high percentage of hydroxyapatite compared to SC (30), but the mineralization can increase significantly during OA development, contributing further to superficial cartilage lesions and more subchondral bone damage, promoting a potentially vicious feedback cycle (31). As conventional MRI

sequences do not have enough contrast to study the OCJ region, the development and constant improvement of this new sequence is of critical importance.

This study had a number of limitations. First, we had a small sample size since our objective was to show the sequence's feasibility as applied to phantoms and in vivo study. Second, despite the high OCJ contrast in the 3D DIR-UTE Cones imaging, the spatial resolution (e.g., slice thickness = 2.2 mm) was still a limiting factor considering the SNR performance of the coils and MRI scanners currently available. Since the OCJ region is comprised of structures that are on the order of microns and millimeters in size, its detailed study will require further improvements regarding MRI resolution. Third, the scan time was still relatively long, though this may be improved with the recent development of parallel imaging and compressed sensing techniques (32).

In conclusion, we showed that the 3D DIR-UTE Cones sequence can be used to image the OCJ of the knee in vivo, highlighting the OCJ with higher CNR in comparison to the previous developed IR-FS-UTE-Cones sequence.

## Supplementary Material

Refer to Web version on PubMed Central for supplementary material.

## Acknowledgements

The authors acknowledge grant support from NIH (R21AR075851) and GE healthcare.

## Abbreviations:

| | |
|---|---|
| **OCJ** | Osteochondral Junction |
| **UTE** | Ultra Short Echo Time |
| **DIR** | Dual Inversion Recovery |
| **CNR** | Contrast to Noise Ratio |
| **BF** | Bone Marrow Fat |
| **SC** | Superficial Cartilage |
| **YLD** | Years Lived with Disability |
| **OA** | Osteoarthritis |

## References

1. James SL, Abate D, Abate KH, Abay SM, Abbafati C, Abbasi N, et al. Global, regional, and national incidence, prevalence, and years lived with disability for 354 diseases and injuries for 195 countries and territories, 1990–2017: a systematic analysis for the Global Burden of Disease Study 2017. The Lancet. 2018;392(10159):1789–858.
2. Sebbag E, Felten R, Sagez F, Sibilia J, Devilliers H, Arnaud L. The world-wide burden of musculoskeletal diseases: a systematic analysis of the World Health Organization Burden of

Diseases Database. Annals of the Rheumatic Diseases. 2019;78(6):844–8. doi: 10.1136/annrheumdis-2019-215142. [PubMed: 30987966]

3. Kloppenburg M, Berenbaum F. Osteoarthritis year in review 2019: epidemiology and therapy. Osteoarthritis and Cartilage. 2020;28(3):242–8. [PubMed: 31945457]
4. Goldring MB, Berenbaum F. Emerging targets in osteoarthritis therapy. Current Opinion in Pharmacology. 2015;22:51–63. doi: 10.1016/j.coph.2015.03.004. [PubMed: 25863583]
5. Lyons TJ, McClure SF, Stoddart RW, McClure J. The normal human chondro-osseous junctional region: evidence for contact of uncalcified cartilage with subchondral bone and marrow spaces. BMC Musculoskeletal Disorders. 2006;7(1):52. doi: 10.1186/1471-2474-7-52. [PubMed: 16787529]
6. Burr DB, Gallant MA. Bone remodelling in osteoarthritis. Nature Reviews Rheumatology. 2012;8(11):665. [PubMed: 22868925]
7. Walsh DA, McWilliams DF, Turley MJ, Dixon MR, Fransès RE, Mapp PI, et al. Angiogenesis and nerve growth factor at the osteochondral junction in rheumatoid arthritis and osteoarthritis. Rheumatology. 2010;49(10):1852–61. [PubMed: 20581375]
8. Suri S, Gill SE, de Camin SM, McWilliams DF, Wilson D, Walsh DA. Neurovascular invasion at the osteochondral junction and in osteophytes in osteoarthritis. Annals of the rheumatic diseases. 2007;66(11):1423–8. [PubMed: 17446239]
9. Pan J, Wang B, Li W, Zhou X, Scherr T, Yang Y, et al. Elevated cross-talk between subchondral bone and cartilage in osteoarthritic joints. Bone. 2012;51(2):212–7. [PubMed: 22197997]
10. Hwang J, Bae WC, Shieu W, Lewis CW, Bugbee WD, Sah RL. Increased hydraulic conductance of human articular cartilage and subchondral bone plate with progression of osteoarthritis. Arthritis & Rheumatism: Official Journal of the American College of Rheumatology. 2008;58(12):3831–42.
11. Emery CA, Whittaker JL, Mahmoudian A, Lohmander LS, Roos EM, Bennell KL, et al. Establishing outcome measures in early knee osteoarthritis. Nature Reviews Rheumatology. 2019;15(7):438–48. [PubMed: 31201386]
12. Roemer FW, Demehri S, Omoumi P, Link TM, Kijowski R, Saarakkala S, et al. State of the Art: Imaging of Osteoarthritis—Revisited 2020. Radiology. 2020:192498.
13. Bae WC, Dwek JR, Znamirowski R, Statum SM, Hermida JC, D'Lima DD, et al. Ultrashort echo time MR imaging of osteochondral junction of the knee at 3 T: identification of anatomic structures contributing to signal intensity. Radiology. 2010;254(3):837–45. [PubMed: 20177096]
14. Bae WC, Biswas R, Chen K, Chang EY, Chung CB. UTE MRI of the osteochondral junction. Current radiology reports. 2014;2(2):35. [PubMed: 25061547]
15. Robson MD, Gatehouse PD, Bydder M, Bydder GM. Magnetic resonance: an introduction to ultrashort TE (UTE) imaging. Journal of computer assisted tomography. 2003;27(6):825–46. [PubMed: 14600447]
16. Du J, Takahashi AM, Bae WC, Chung CB, Bydder GM. Dual inversion recovery, ultrashort echo time (DIR UTE) imaging: creating high contrast for short-T2 species. Magnetic Resonance in Medicine: An Official Journal of the International Society for Magnetic Resonance in Medicine. 2010;63(2):447–55.
17. Lee YH, Kim S, Song H-T, Kim I, Suh J-S. Weighted subtraction in 3D ultrashort echo time (UTE) imaging for visualization of short T2 tissues of the knee. Acta radiologica. 2014;55(4):454–61. [PubMed: 23934936]
18. Du J, Carl M, Bae WC, Statum S, Chang EY, Bydder GM, et al. Dual inversion recovery ultrashort echo time (DIR-UTE) imaging and quantification of the zone of calcified cartilage (ZCC). Osteoarthritis Cartilage. 2013;21(1):77–85. Epub 2012/10/03. doi: 10.1016/j.joca.2012.09.009. [PubMed: 23025927]
19. Mackay JW, Low SBL, Houston GC, Toms AP. Ultrashort TE evaluation of the osteochondral junction in vivo: a feasibility study. The British Journal of Radiology. 2016;89(1059):20150493. doi: 10.1259/bjr.20150493.
20. Ma YJ, Jerban S, Carl M, Wan L, Guo T, Jang H, et al. Imaging of the region of the osteochondral junction (OCJ) using a 3D adiabatic inversion recovery prepared ultrashort echo time cones (3D IR-UTE-cones) sequence at 3 T. NMR in Biomedicine. 2019;32(5):e4080. [PubMed: 30794338]

21. Kühn J-P, Hernando D, Meffert PJ, Reeder S, Hosten N, Laqua R, et al. Proton-density fat fraction and simultaneous R2* estimation as an MRI tool for assessment of osteoporosis. European radiology. 2013;23(12):3432–9. [PubMed: 23812246]
22. Lu A, Daniel BL, Pauly JM, Butts Pauly K. Improved slice selection for R2* mapping during cryoablation with eddy current compensation. Journal of Magnetic Resonance Imaging: An Official Journal of the International Society for Magnetic Resonance in Medicine. 2008;28(1):190–8.
23. Carl M, Bydder GM, Du J. UTE imaging with simultaneous water and fat signal suppression using a time-efficient multispoke inversion recovery pulse sequence. Magnetic resonance in medicine. 2016;76(2):577–82. [PubMed: 26309221]
24. Ma Y-J, Lu X, Carl M, Zhu Y, Szeverenyi NM, Bydder GM, et al. Accurate T1 mapping of short T2 tissues using a three-dimensional ultrashort echo time cones actual flip angle imaging-variable repetition time (3D UTE-Cones AFI-VTR) method. Magnetic Resonance in Medicine. 2018;80(2):598–608. doi: 10.1002/mrm.27066. [PubMed: 29314235]
25. Ma Y-J, Zhao W, Wan L, Guo T, Searleman A, Jang H, et al. Whole knee joint T1 values measured in vivo at 3T by combined 3D ultrashort echo time cones actual flip angle and variable flip angle methods. Magnetic Resonance in Medicine. 2019;81(3):1634–44. doi: 10.1002/mrm.27510. [PubMed: 30443925]
26. Ma YJ, Jerban S, Jang H, Chang EY, Du J. Fat suppression for ultrashort echo time imaging using a novel soft-hard composite radiofrequency pulse. Magnetic resonance in medicine. 2019;82(6):2178–87. [PubMed: 31317565]
27. Manhard MK, Horch RA, Gochberg DF, Nyman JS, Does MD. In Vivo Quantitative MR Imaging of Bound and Pore Water in Cortical Bone. Radiology. 2015;277(1):221–9. Epub 2015/05/29. doi: 10.1148/radiol.2015140336. [PubMed: 26020434]
28. Suri S, Walsh DA. Osteochondral alterations in osteoarthritis. Bone. 2012;51(2):204–11. [PubMed: 22023932]
29. Mapp PI, Walsh DA. Mechanisms and targets of angiogenesis and nerve growth in osteoarthritis. Nature Reviews Rheumatology. 2012;8(7):390. [PubMed: 22641138]
30. Zhang Y, Wang F, Tan H, Chen G, Guo L, Yang L. Analysis of the mineral composition of the human calcified cartilage zone. International journal of medical sciences. 2012;9(5):353. [PubMed: 22811609]
31. Ferguson VL, Bushby AJ, Boyde A. Nanomechanical properties and mineral concentration in articular calcified cartilage and subchondral bone. Journal of Anatomy. 2003;203(2):191–202. [PubMed: 12924819]
32. Ma Y-J, Searleman AC, Jang H, Wong J, Chang EY, Corey-Bloom J, et al. Whole-brain myelin imaging using 3D double-echo sliding inversion recovery ultrashort echo time (DESIRE UTE) MRI. Radiology. 2020;294(2):362–74. [PubMed: 31746689]

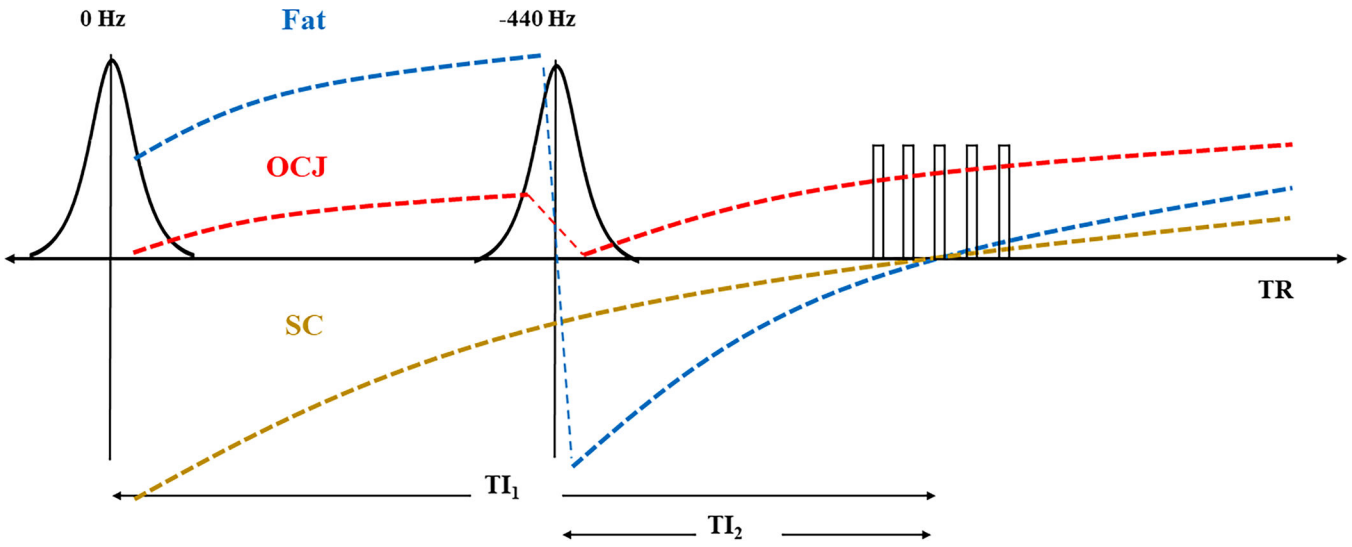


**Figure 1.**

DIR-UTE sequence diagram. The DIR-UTE sequence utilizes two adiabatic IR pulses with center frequencies of 0 and −440 Hz (fat frequency offset at 3T) to invert long T2 water and fat, respectively. These IR pulses have a relatively narrow bandwidth of around 500 Hz. TIs were determined experimentally to reach the nulling point at the same time of data acquisition. At the optimized $TI_1$ and $TI_2$ in this DIR-UTE sequence, superficial layers of cartilage (SC) and fat can both be suppressed simultaneously. The OCJ signal was largely saturated when the second IR preparation pulse was applied due to its short T2 relaxation time compared to the relatively long relaxation times of the adiabatic IR pulses. The relatively high signals from the OCJ were acquired with a train of UTE spokes (i.e., 21 used in this study) at the signal nulling point of SC and fat. Hard pulse excitation was applied to reduce eddy current effects. Both RF and gradient spoiling were used to crush the residual transverse magnetizations after acquisition in each UTE spoke.

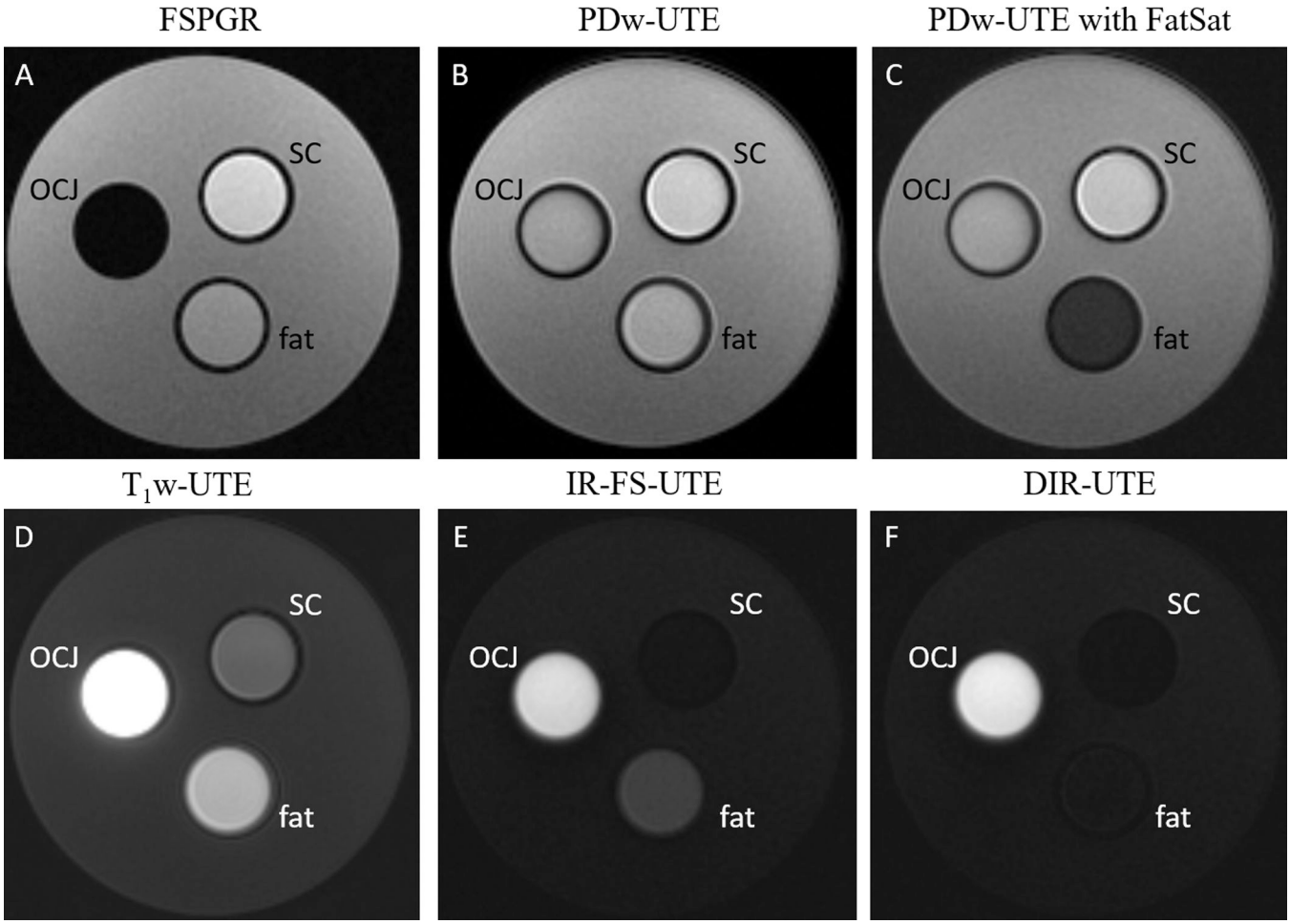


**Figure 2.**

Phantom study. (A-F) A phantom consisting of three tubes with vegetable oil (simulating fat), distilled water with 0.015 g/L of $MnCl_2$ (simulating the superficial layer of cartilage (SC)), and distilled water with 3.6 g/L of $MnCl_2$ (simulating the osteochondral junction (OCJ)), all in agarose gel. (A) Fast spoiled gradient echo (FSPGR) sequence showing low signal from the OCJ due to fast signal decay. PDw-UTE Cones without (B) and with FatSat (C) can detect signals from the OCJ and SC, with low contrast between the two. (D) $T_{1w}$-UTE Cones sequence shows higher signal intensities in both the OCJ and fat tubes due to their relatively short $T_1$s. (E) IR-FS-UTE Cones shows effective SC signal suppression but is less effective in fat signal suppression. (F) DIR-UTE Cones sequence shows the OCJ contrast with better suppression of signal from fat as compared to the IR-FS-UTE Cones (E) sequence.

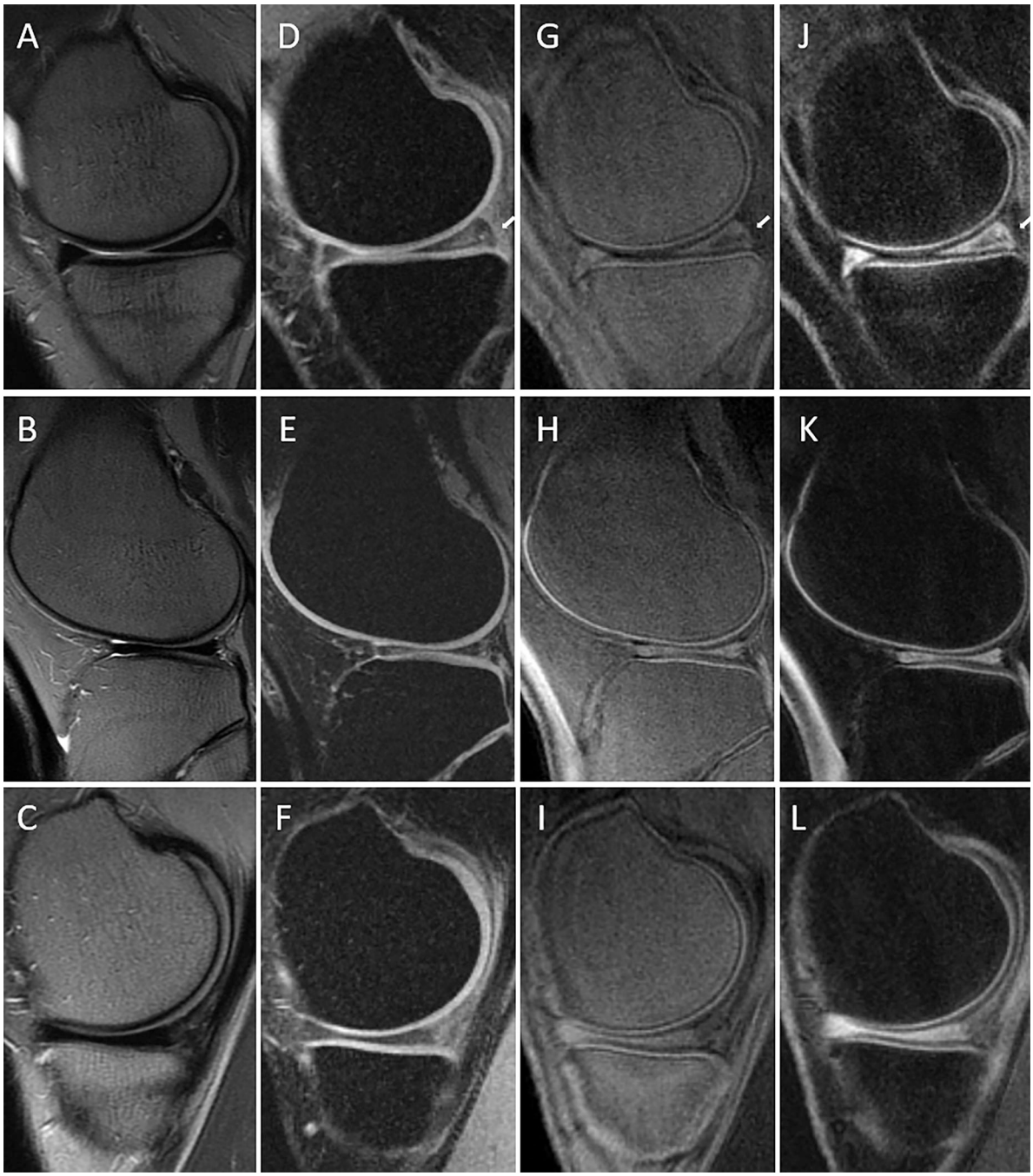


**Figure 3.**

Volunteer study. $T_{2w}$-FSE (A, B, C), FSPGR (D, E, F), IR-FS-UTE Cones (G, H, I), and DIR-UTE Cones (J, L, M) sequences performed in the knee joints of two healthy volunteers (the first row represents the first volunteer (38 years old male), while the second and third rows represent the second volunteer (38 years old male). On $T_{2w}$-FSE and FSPGR images, the signal in the osteochondral junction (OCJ) region cannot be effectively detected due to its fast signal decay. (G-I) IR-FS-UTE Cones sequences highlighting the OCJ and suppressing the superficial layer of cartilage and the subchondral bone. (J-L) DIR-UTE

Cones sequences highlights the OCJ region with better subchondral bone fat suppression than the IR-FS-UTE Cones can. Note degenerative changes in the posterior horn of medial meniscus (small arrows in D,G, J) in the first volunteer.

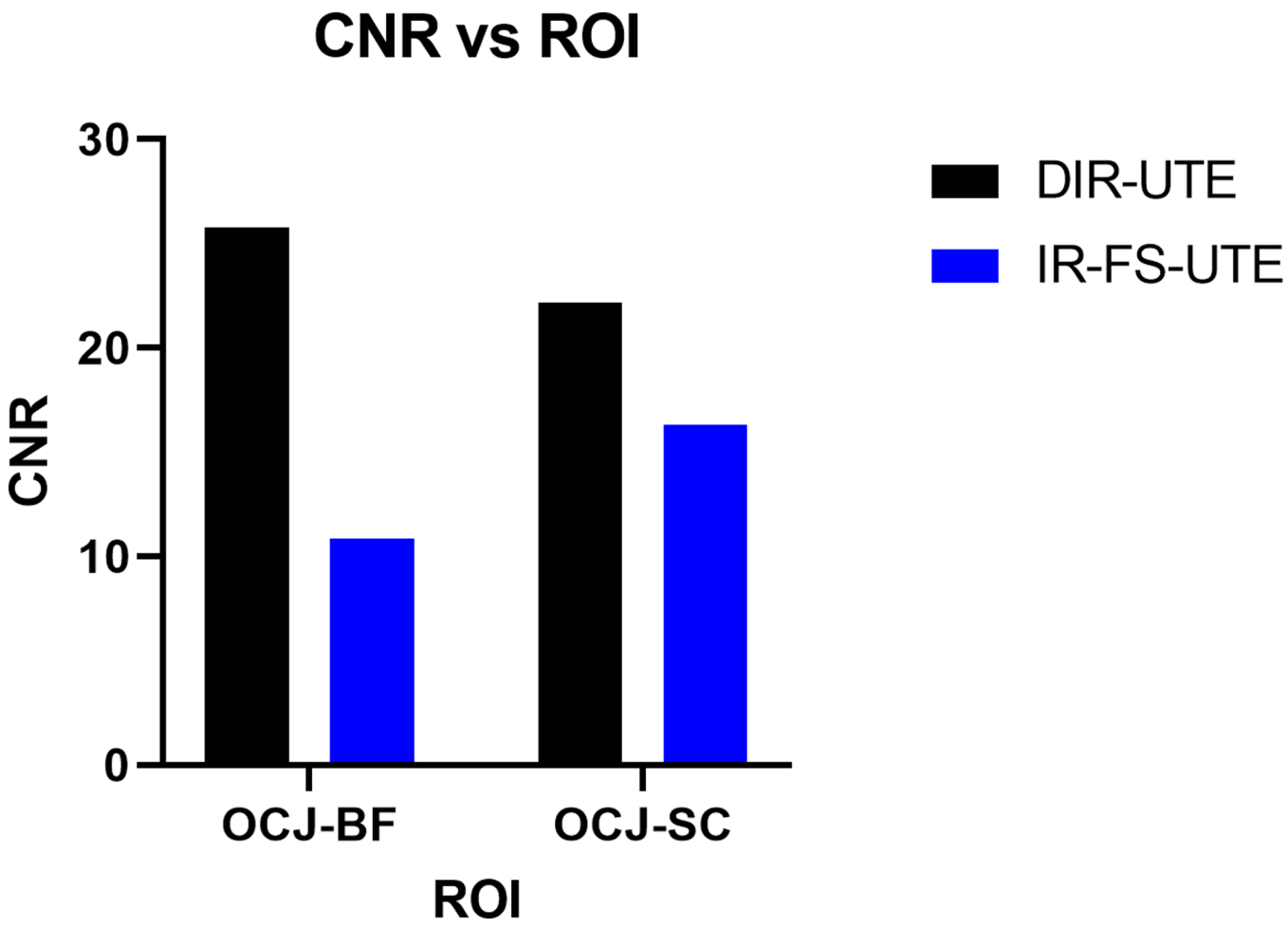


**Figure 4.**

Bar plot of the contrast-to-noise ratios (CNRs) between the osteochondral junction (OCJ) and subchondral bone fat (BF) (OCJ-BF) and the OCJ and superficial layer of cartilage (SC) (OCJ-SC), using the 3D DIR-UTE (black bars) and IR-FS-UTE sequences (blue bars) in the study of four volunteers. The 3D DIR-UTE Cones sequence shows a higher CNR between the OCJ and BF (mean, standard deviation (SD): 25.7 ± 2.3) and between the OCJ and SC (mean, SD: 22.2 ± 3.5) compared to the IR-FS-UTE sequence (mean, SD: 10.8 ± 2.5 and 16.3 ± 2.6, respectively).


**Figure 5.**

Images from $T_{2w}$-FSE (A, B), FSPGR (C, D), IR-FS-UTE Cones (E, F), and DIR-UTE Cones (G, H) performed in the knees of two patients with osteoarthritis (first row represents the first patient (50 years old male) and second row represents the second patient (48 years old male)). Cartilage thinning can be seen on the weight-bearing area of the medial compartment in the first patient (arrows in A, C, E, G) and on the trochlea in the second patient (open arrows in B, D, F, H). Note the interruption of the bright line representing the osteochondral junction on both IR-FS-UTE Cones and DIR-UTE Cones images (E, F, G, H). The 3D DIR-UTE Cones sequence (G and H) is more efficient in suppressing the subchondral bone fat than the IR-FS-UTE Cones (E, F).

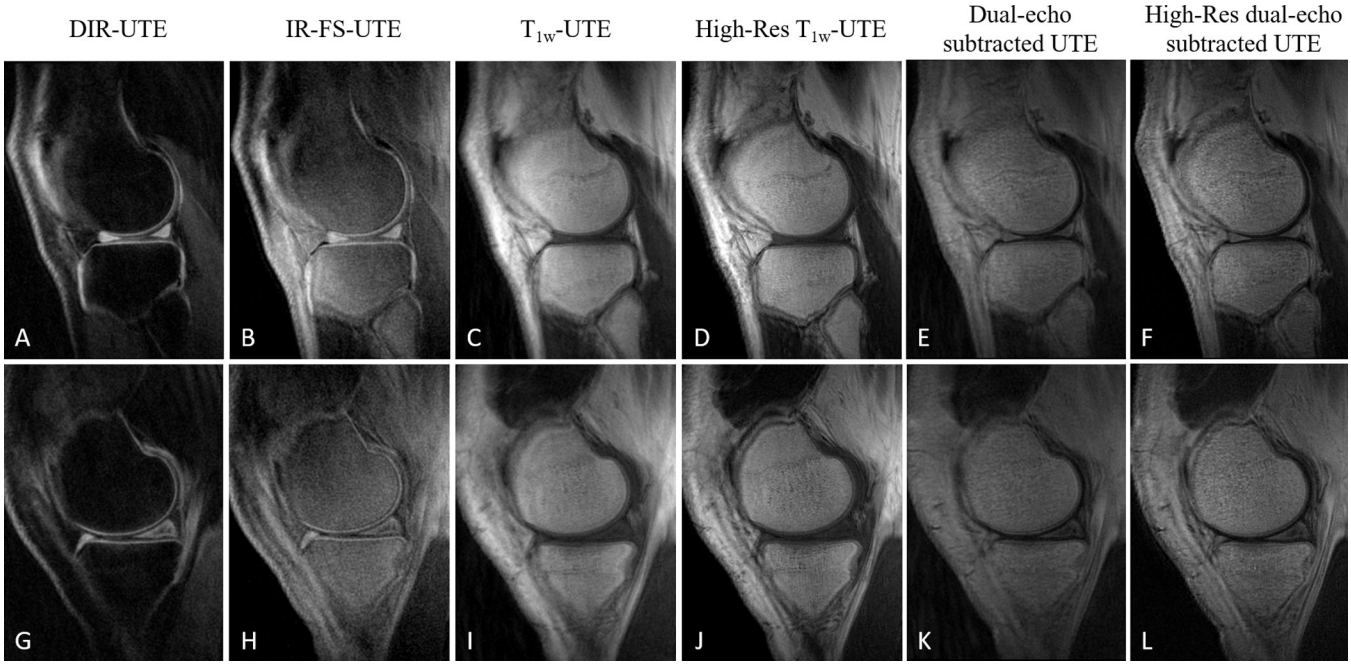


**Figure 6.**

Comparison study including DIR-UTE Cones (A and G), IR-FS-UTE Cones (B and H), low (C and I) and high (D and J) resolution $T_{1w}$-UTE, low (E and K) and high (F and L) dual-echo subtracted UTE images performed in the knee joint of a healthy volunteer (38 years old male) on both the lateral (first row) and medial (second row) compartments. The images on higher resolution $T_{1w}$-UTE and dual-echo subtracted UTE present thinner OCJ structure and higher SNR compared to DIR-UTE and IR-FS-UTE. However, the BF persists with high signals in both $T_{1w}$-UTE and dual-echo subtracted UTE images, which decreases the contrast between the OCJ and BF. The DIR-UTE and IR-FS-UTE sequences offer higher contrast between the OCJ, SC, and BF, with the DIR-UTE providing particularly notable contrast.

**Table 1.**

Phantom study imaging parameters.

| | 3D DIR-UTE Cones | 3D IR-FS-UTE Cones | 3D FSPGR | 3D PDw-UTE | 3D $T_{1w}$-UTE |
|---|---|---|---|---|---|
| FOV | 14 × 14 × 10.8 $cm^3$ | 14 × 14 × 10.8 $cm^3$ | 14 × 14 × 10.8 $cm^3$ | 14 × 14 × 10.8 $cm^3$ | 14 × 14 × 10.8 $cm^3$ |
| Matrix | 256 × 256 × 36 | 256 × 256 × 36 | 256 × 256 × 36 | 256 × 256 × 36 | 256 × 256 × 36 |
| Slice thickness | 2.2 mm | 2.2 mm | 2.2 mm | 3 mm | 3 mm |
| Bandwidth | 250 kHz | 250 kHz | 250 kHz | 250 kHz | 250 kHz |
| $TI_1/TI_2$ | 400/160 ms | 400 ms | | | |
| TR | 1200 ms | 1200 ms | 5.6 ms | 10 ms | 10 ms |
| TE | 0.032 ms | 0.032 ms | 2.4 ms | 0.032 ms | 0.032 ms |
| FA | 10° | 10° | 4° | 4° | 30° |
| $N_{sp}$ | 21 | 21 | | | |
| $\tau$ | 5 ms | 5 ms | | | |
| Total scan time | 5 min 30 sec | 5 min 30 sec | 48 sec | 1 min 48 sec | 1 min 48 sec |

FOV: field-of-view; TR: repetition time; TI: time of inversion recovery; TE: echo time; FA: flip angle; $N_{sp}$: number of spokes; $\tau$: time between spokes; FSPGR: fast spoiled gradient echo; IR: inversion recovery; FS: fat saturation; PD: proton density

**Table 2.**

In vivo study imaging parameters.

| | 3D DIR-UTE Cones | 3D IR-FS-UTE Cones | 3D FSPGR with fat saturation | 2D $T_{2w}$-FSE with fat saturation |
|---|---|---|---|---|
| FOV | 14 × 14 × 8.8 $cm^3$ | 14 × 14 × 8.8 $cm^3$ | 14 × 14 × 8.8 $cm^3$ | 14 × 14 × 8.8 $cm^3$ |
| Matrix | 256 × 256 × 40 | 256 × 256 × 40 | 256 × 256 × 40 | 352 × 256 × 40 |
| Slice thickness | 2.2 mm | 2.2 mm | 2.2 mm | 3 mm |
| Bandwidth | 250 kHz | 250 kHz | 125 kHz | 82.3 kHz |
| $TI_1/TI_2$ | 520/180 ms | 600 ms | | |
| TR | 1200 ms | 1200 ms | 5.6 ms | 5086 ms |
| TE | 0.032 ms | 0.032 ms | 2.4 ms | 71 ms |
| FA | 10° | 10° | 4° | 90° |
| $N_{sp}$ | 21 | 21 | | |
| $\tau$ | 5 ms | 5 ms | | |
| Total scan time | 9 min 54 sec | 9 min 55 sec | 1 min 12 sec | 2 min |

FOV: field-of-view; TR: repetition; TI: time of inversion recovery; TE: echo time; FA: flip angle; $N_{sp}$: number of spokes; $\tau$: time between spokes; FSPGR: fast spoiled gradient echo; IR: inversion recovery; FS: fat saturation

**Table 3.**

3D $T_{1w}$-UTE and dual-echo UTE sequence parameters for the in vivo comparison study.

| | **3D $T_{1w}$-UTE** | **High-Resolution 3D $T_{1w}$-UTE** | **3D dual-echo UTE** | **High-Resolution 3D dual-echo UTE** |
|---|---|---|---|---|
| FOV | 14 × 14 × 8.8 $cm^3$ | 14 × 14 × 8.4 $cm^3$ | 14 × 14 × 8.8 $cm^3$ | 14 × 14 × 8.4 $cm^3$ |
| Matrix | 256 × 256 × 40 | 340 × 340 × 56 | 256 × 256 × 40 | 340 × 340 × 56 |
| Slice thickness | 2.2 mm | 1.5 mm | 2.2 mm | 1.5 mm |
| Bandwidth | 250 kHz | 250 kHz | 250 kHz | 250 kHz |
| TR | 10 ms | 10 ms | 9.3 ms | 9.8 ms |
| TE | 0.032 ms | 0.032 ms | 0.032/4.4 ms | 0.032/4.4 ms |
| FA | 30° | 30° | 10° | 10° |
| Oversampling factor | 1 | 1.5 | 1 | 1.54 |
| Total scan time | 2 min 11 sec | 9 min 30 sec | 2 min 3 sec | 9 min 34 sec |

FOV: field-of-view; TR: repetition time; TE: echo time; FA: flip angle